XI International Conference on Computational Plasticity. Fundamentals and Applications
COMPLAS XI
E. Oñate, D.R.J. Owen, D. Peric and B. Suárez (Eds)

NUMERICAL ANALYSIS OF PULSATILE BLOOD FLOW IN REALISTIC CORONARY BYPASS MODELS

JAN VIMMR*, ALENA JONÁŠOVÁ* AND ONDŘEJ BUBLÍK*

*University of West Bohemia, Department of Mechanics
Univerzitni 22, CZ-306 14 Pilsen, Czech Republic
e-mail: jvimmr@kme.zcu.cz

Key words: Aorto-coronary Bypass, End-to-side Anastomosis, Side-to-side Anastomosis, Hemodynamics, Pulsatile Flow, FVM

Abstract. The paper's objective lies in numerical modelling of pulsatile blood flow in complete aorto-coronary bypass models reconstructed from CT data, especially in models with individual and sequential bypass grafts. Unsteady blood flow is described by the nonlinear system of the incompressible Navier-Stokes equations in 3D, which is numerically solved using developed computational algorithm based on the fully implicit projection method and on the cell-centred finite volume method for hybrid unstructured tetrahedral grids. Obtained numerical results are discussed with regard to distribution of velocity, wall shear stress and oscillatory shear index at proximal and distal anastomoses, i.e., in areas prone to development of intimal hyperplasia.

1 INTRODUCTION

According to the most recent European cardiovascular disease statistics[1] almost half of affected people had either brain stroke or heart infarction. Considering also the increasing number of patients and surgical treatments connected with stenosed or occluded arteries, the understanding of cardiovascular disease origin and development is crucial for its future prevention and treatment. In the case of ischemic heart disease, one of possible surgical interventions is the implantation of venous bypass grafts, often creating a detour between aorta and the damaged coronary artery branch. The failure rate of implanted bypass grafts is mostly related to the development of intimal hyperplasia, an abnormal healing process in the anastomosis region. It is typical for the thickening of tunica intima leading to decrease in the arterial lumen and consequently to graft failure[2]. Nowadays atherosclerosis and intimal hyperplasia alike are hypothesized to be triggered by non-uniform hemodynamics leading to morphological and metabolic changes within the vessel wall[3]. Recirculation zones and low and oscillating wall shear stress are some of the supposed triggering factors that are responsible for endothelium activation[4]. Beside

clinical research, numerical investigation of bypass hemodynamics represents a valuable insight into the problem and provide so better understanding of blood flow influence on cardiovascular disease occurrence and development.

The objective of this paper is the modelling of pulsatile blood flow in patient-specific aorto-coronary bypass models with emphasis placed on the hemodynamics study in individual and sequential types. We denote the individual type as the bypass with one proximal and one distal (end-to-side) anastomosis and the sequential type as the one with one proximal and two distal (side-to-side and end-to-side) anastomoses. As is apparent from the presence of multiple anastomoses, the sequential bypass technique is often employed to connect several coronary arteries by one graft. However, a major unknown of such bypasses lies in the resulting blood supply to each connected coronary artery and the possibility of intimal hyperplasia formation at one or both established anastomoses. In this regard, we perform a numerical analysis of pulsatile blood flow in two aorto-coronary bypass models reconstructed from CT data provided by the University Hospital Pilsen, Czech Republic. For results discussion, special emphasis is placed on the evaluation and analysis of main hemodynamic factors such as distribution of velocity, wall shear stress (WSS) and oscillatory shear index (OSI) in areas that may be prone to development of intimal hyperplasia.

2 PROBLEM FORMULATION AND BYPASS MODELS

In comparison to other published papers, which mostly dealt with distal bypass parts, especially the distal anastomosis[5], the present study considers complete aorto-coronary bypass models with realistic geometry, i.e., both proximal and distal anastomoses are modelled. In this way, the problem of boundary conditions may be adequately approached. In human vessels, blood behaves as an incompressible non-Newtonian fluid. As is shown in other studies[6], blood's shear-thinning behaviour may be neglected in selected cases such

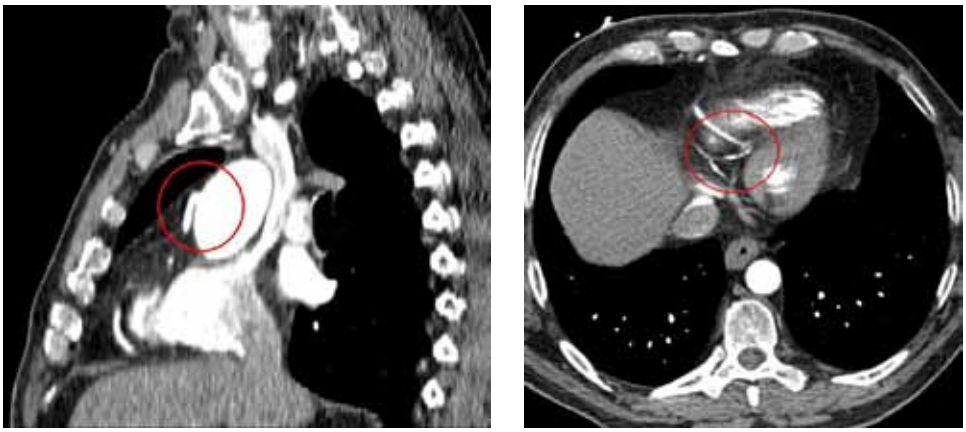

Figure 1: CT scans of individual aorto-coronary bypass model – position of the proximal end-to-side anastomosis (*left*) and the distal end-to-side anastomosis (*right*)

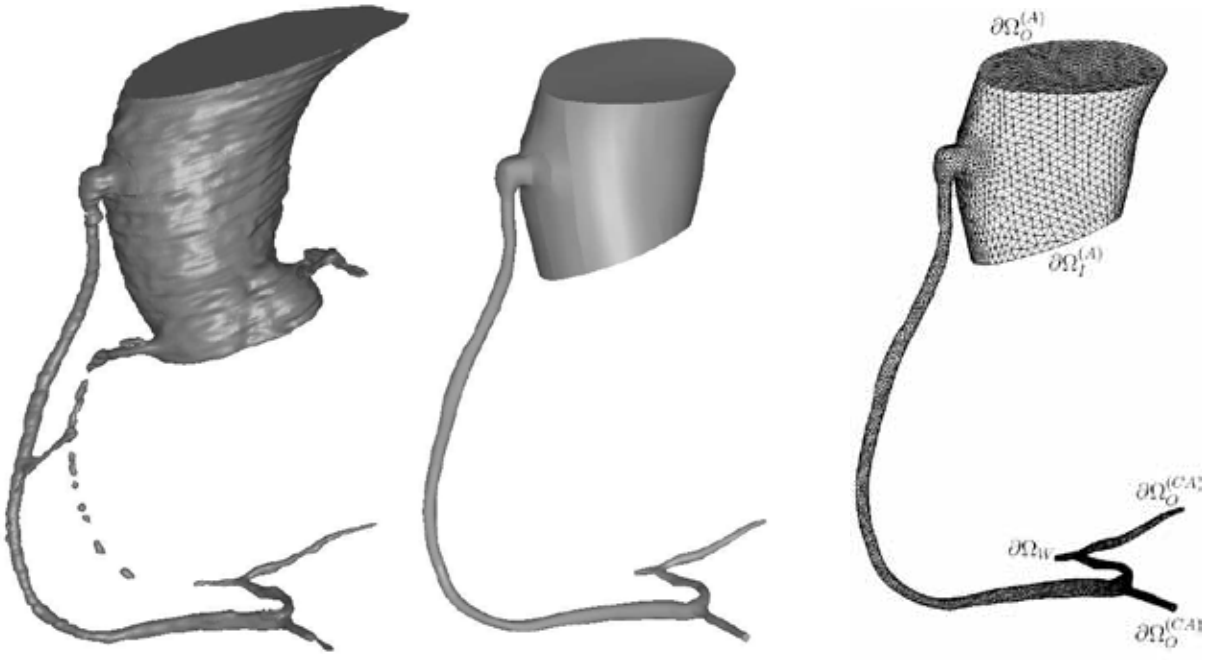

Figure 2: Individual aorto-coronary bypass model – (*from left to right*) primary reconstruction from CT data, model after smoothing, tetrahedral computational mesh with denoted computational domain boundaries

as in human aorta. Furthermore, previous numerical simulations of steady non-Newtonian blood flow performed by the authors of this paper in an idealized coronary bypass model[7] showed negligible non-Newtonian effects. Therefore, in the present study, blood's complex rheological properties are neglected and blood is assumed to be an Newtonian fluid. Further, all numerical simulations of pulsatile blood flow are carried out for bypass models with rigid and impermeable walls. The authors are aware that this assumption, especially in connection with the elastic aorta, represents a relevant limitation of the current mathematical model. However, an improvement in relation to vessel compliance is planned in one of their future studies.

For the purpose of the present study, two sets of CT data were provided by the University Hospital Pilsen, Czech Republic. The first data set contained the CT scans of an individual graft, Fig. 1, whose proximal end was attached to the aorta and the distal one was sewn to an occluded branch of coronary arteries. The corresponding primary model after reconstruction in software Amira is shown in Fig. 2 together with the final smoothed model and the unstructured tetrahedral computational mesh, which was generated in the system Altair Hypermesh. Fig. 3 gives a detailed view at the mesh in the distal anastomosis region and in the pre-anastomosis coronary bifurcation. For this bypass type, following inlet and outlet boundary conditions are prescribed, see boundaries denoted in Fig. 2,

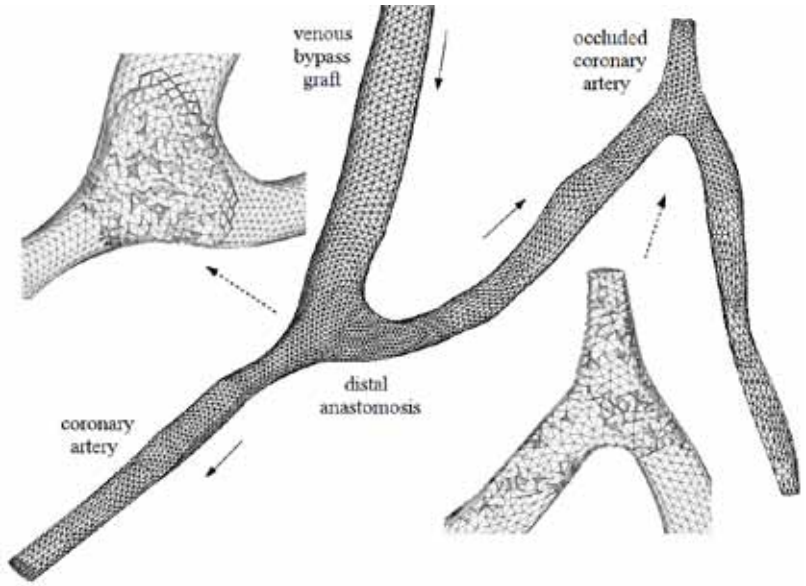

Figure 3: Individual aorto-coronary bypass model – view at the distal end-to-side anastomosis region with coronary bifurcation

- aorta inlet $\partial\Omega_I^{(A)}$ and aorta outlet $\partial\Omega_O^{(A)}$ – time-dependent flow rate $Q(t)$ and pressure $p(t)$, respectively, are applied. The values of flow rate and pressure are taken from literature[8], Fig. 4;
- coronary artery outlet $\partial\Omega_O^{(CA)}$ – constant pressure equal to average arterial pressure 12 000 Pa is given;
- occluded coronary artery is treated as a rigid wall boundary $\partial\Omega_W$.

In order to perform numerical computations with non-dimensional primitive variables, reference values have to be set. For the individual graft, the reference velocity $U_{ref}^{(1)}$ is

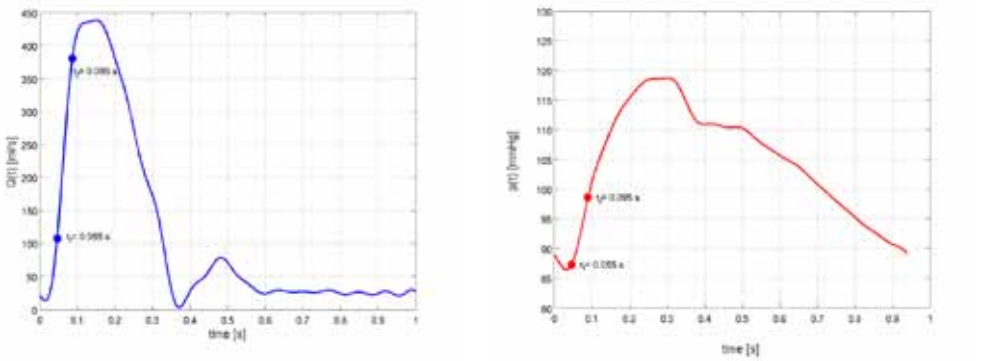

Figure 4: Individual aorto-coronary bypass model – time-dependent flow rate $Q(t)$ prescribed at the aorta inlet $\partial\Omega_I^{(A)}$ (*left*) and time-dependent pressure $p(t)$ prescribed at the aorta outlet $\partial\Omega_O^{(A)}$ (*right*)

chosen to be equal to $0.1592\,\mathrm{m}\cdot\mathrm{s}^{-1}$, corresponding to average aorta inlet flow rate, Fig. 4 (*left*), and the reference diameter is $D_{ref}^{(1)} = 0.036\,\mathrm{m}$, corresponding to average aorta diameter. According to prescribed boundary conditions[8], blood's density and viscosity are considered to be constant $\eta^{(1)} = 0.0049\,\mathrm{Pa}\cdot\mathrm{s}$ and $\varrho^{(1)} = 1055\,\mathrm{kg}\cdot\mathrm{m}^{-3}$, respectively.

The second set of provided CT scans contained data of a sequential aorto-coronary bypass with one side-to-side anastomosis and one end-to-side anastomosis, Fig. 5. The figure shows the reconstructed bypass model and the unstructured tetrahedral computational mesh as well. Detailed view at both the side-to-side and end-to-side anastomoses is given in Fig. 6. Since the authors of this paper have access to physiological data measured within a real side-to-side anastomosis[9], first numerical simulations of pulsatile blood flow in the sequential aorto-coronary bypass model are done for the side-to-side anastomosis

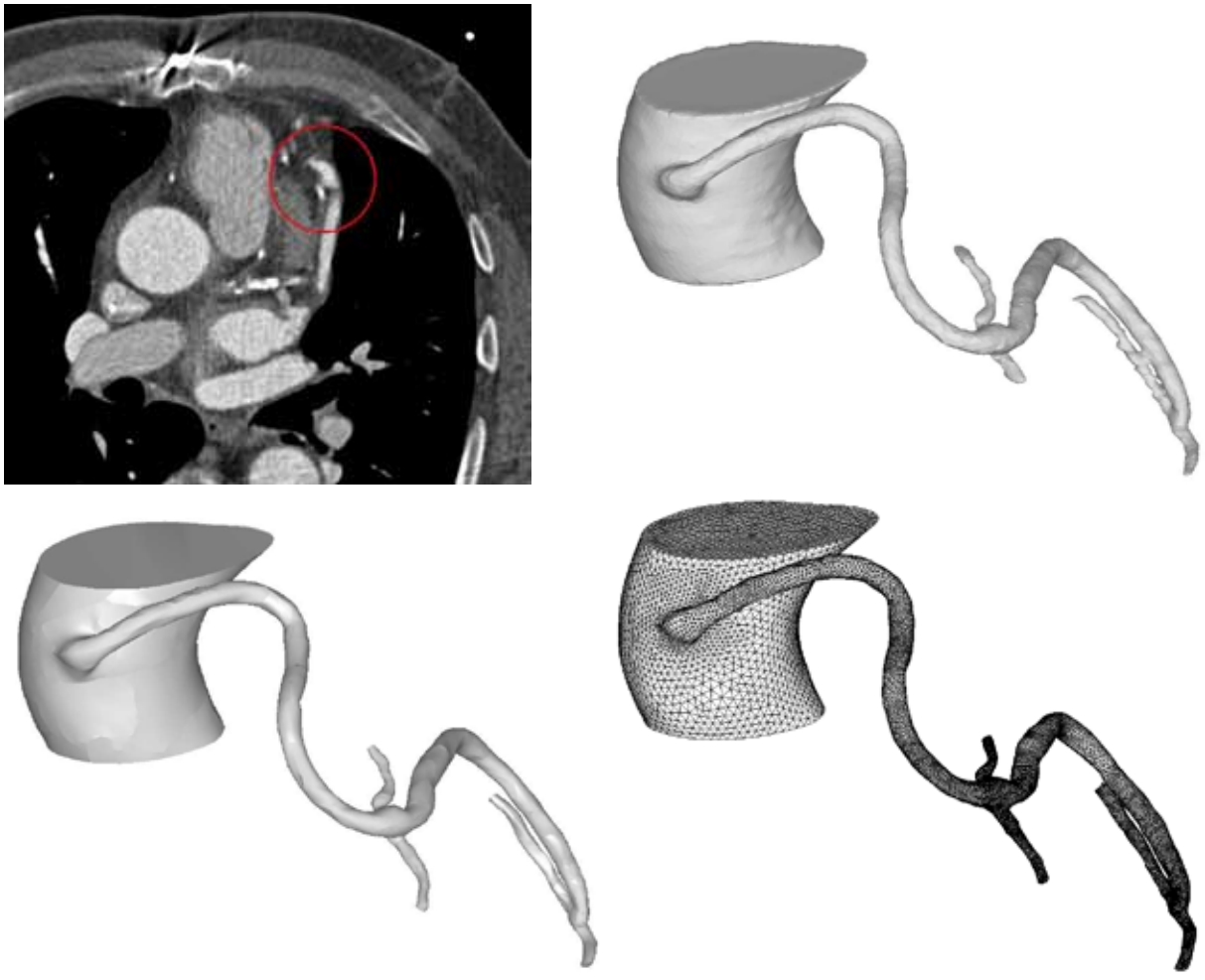

Figure 5: Sequential aorto-coronary bypass model – (*from left to right*) CT scan with denoted position of the side-to-side anastomosis, primary reconstruction from CT data, model after smoothing, tetrahedral computational mesh

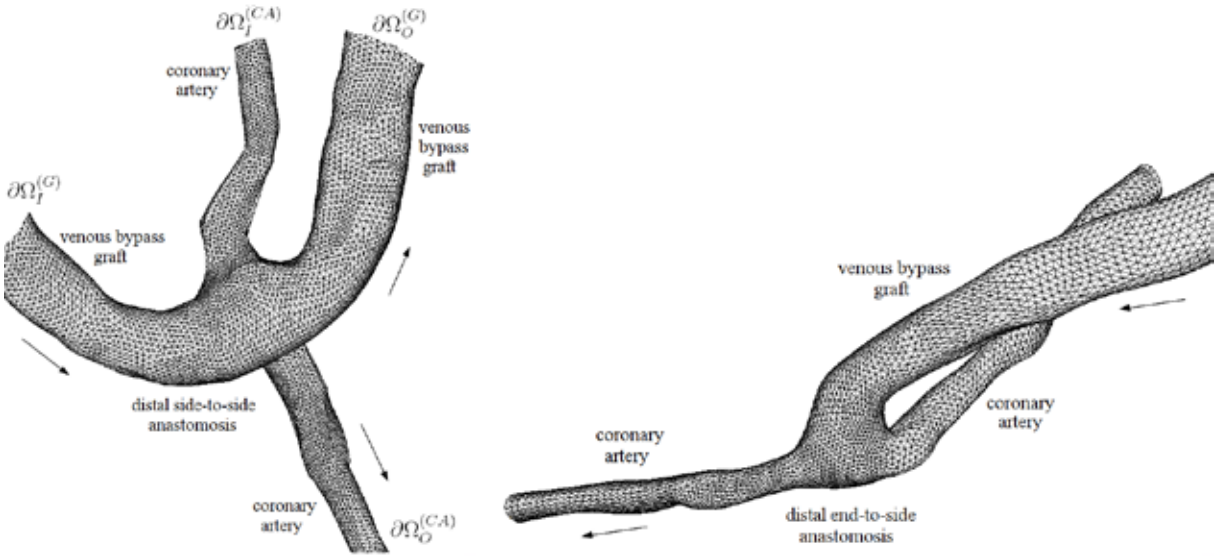

Figure 6: Sequential aorto-coronary bypass model – view at the distal side-to-side anastomosis (*left*) and at the distal end-to-side anastomosis (*right*)

with following inlet and outlet boundary conditions, Fig. 6 (*left*),

- graft inlet $\partial\Omega_I^{(G)}$ and coronary artery inlet $\partial\Omega_I^{(CA)}$ – time-dependent flow rates $Q(t)^{(G)}$ and $Q(t)^{(CA)}$, respectively, are applied according to literature[9], Fig. 7;
- graft outlet $\partial\Omega_O^{(G)}$ and coronary artery outlet $\partial\Omega_O^{(CA)}$ – constant pressure equal to average arterial pressure 12 000 Pa is given.

Similarly to the case of individual graft, reference values have to be chosen. The reference velocity $U_{ref}^{(2)} = 0.1193\,\mathrm{m}\cdot\mathrm{s}^{-1}$ is determined from average graft inlet flow rate, Fig. 7, and the reference diameter $D_{ref}^{(2)} = 0.0045\,\mathrm{m}$ set equal to average graft diameter. According to prescribed values of boundary conditions[9], blood's density and viscosity are $\eta^{(2)} = 0.0037\,\mathrm{Pa}\cdot\mathrm{s}$ and $\varrho^{(2)} = 1060\,\mathrm{kg}\cdot\mathrm{m}^{-3}$, respectively.

3 MATHEMATICAL MODELLING

3.1 Mathematical model

Let us consider a time interval $(0, \mathcal{T})$, $\mathcal{T} > 0$ and a bounded 3D computational domain $\Omega \subset \mathbf{R}^3$ with boundary $\partial\Omega$. According to assumptions established in the previous section, coronary blood flow in this computational domain may be modelled as unsteady laminar isothermal flow of incompressible Newtonian fluid that in the space-time cylinder $\Omega_T = \Omega \times (0, \mathcal{T})$ is mathematically described by the non-linear system of incompressible Navier-

Stokes (NS) equations written in the non-dimensional form as

$$\frac{\partial v_j}{\partial x_j} = 0\,, \tag{1}$$

$$\frac{\partial v_i}{\partial t} + \frac{\partial}{\partial x_j}(v_i v_j) + \frac{\partial p}{\partial x_i} = \frac{1}{\mathrm{Re}^{(s)}} \frac{\partial^2 v_i}{\partial x_j \partial x_j} \quad i,j = 1,2,3, \tag{2}$$

where t is the time, v_i is the i-th component of the velocity vector $\boldsymbol{v} = [v_1, v_2, v_3]^T$ corresponding to the Cartesian component x_i of the space variables vector $\boldsymbol{x} = [x_1, x_2, x_3]^T$, p is the pressure and $\mathrm{Re}^{(s)} = U_{ref}^{(s)} D_{ref}^{(s)} \varrho^{(s)} / \eta^{(s)}$, $s = 1, 2$ is the reference Reynolds number. For the individual aorto-coronary bypass model and for the side-to-side anastomosis model, we get $\mathrm{Re}^{(1)} = 1\,234.3$ and $\mathrm{Re}^{(2)} = 153.8$, respectively.

3.2 Numerical method

The numerical solution of the non-linear time-dependent system of the incompressible NS equations (1) – (2) is based on the fractional step method and the cell-centred finite volume method formulated for hybrid unstructured tetrahedral grids, whose control volume Ω_k is shown in Fig. 8. The principle of hybrid grid systems was proposed by Kim et al.[10] Time discretization of the incompressible NS equations (2) is performed using the implicit second order Crank-Nicolson scheme with linearization of the convective term.

Let us introduce a variable $\delta\hat{v}_i = \hat{v}_i - v_i^n$, where $\hat{v}_i$ is the intermediate velocity and v_i^n is the velocity computed at the time level n. Let us further introduce a pressure correction function Ψ defined as $\Psi = (p^{n+1} - p^n)\Delta t$, where p^{n+1} and p^n are the pressure values computed at the time levels n and $(n+1)$, respectively. After the discretization, we get

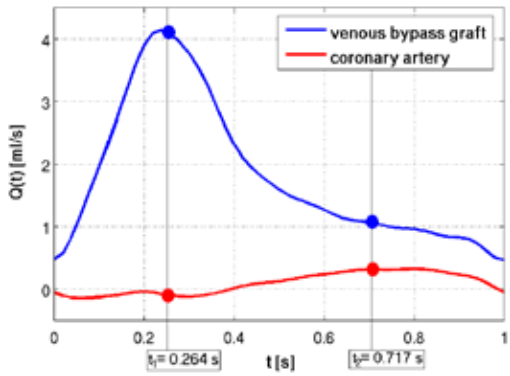

Figure 7: Time-dependent flow rates prescribed at the graft inlet $Q(t)^{(G)}$ and at the coronary artery inlet $Q(t)^{(CA)}$ of the side-to-side anastomosis model

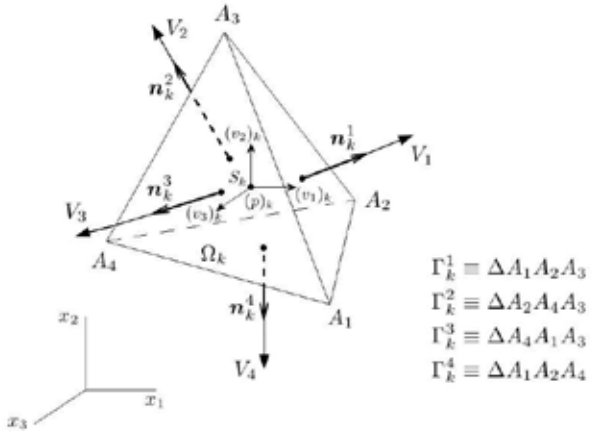

Figure 8: A tetrahedral control volume $\Omega_k = A_1A_2A_3A_4$ with boundary $\partial\Omega_k = \bigcup_{m=1}^{4} \Gamma_k^m$

following system of equations

$$(\delta\hat{v}_i)_k + \frac{\Delta t}{2|\Omega_k|}\sum_{m=1}^{4}\left(\delta\hat{v}_{i\,m}V_m^n + v_{i\,m}^n \cdot {}^j n_k^m \;\delta\hat{v}_{j\,m} + 2v_{i\,m}^n V_m^n\right)|\Gamma_k^m|$$

$$+\frac{\Delta t}{2|\Omega_k|}\sum_{m=1}^{4} p_m^n \cdot {}^i n_k^m\,|\Gamma_k^m| = \frac{\Delta t}{2\mathrm{Re}^{(s)}|\Omega_k|}\sum_{m=1}^{4}\frac{\partial}{\partial \boldsymbol{n}_k^m}\left(\delta\hat{v}_{i\,m} + 2v_{i\,m}^n\right)|\Gamma_k^m|\,, \tag{3}$$

$$(\hat{v}_i)_k = (v_i^n)_k + (\delta\hat{v}_i)_k, \tag{4}$$

$$\sum_{m=1}^{4}\frac{\partial\Psi}{\partial \boldsymbol{n}_k^m}|\Gamma_k^m| = \sum_{m=1}^{4}\hat{v}_{i\,m}\cdot {}^i n_k^m\,|\Gamma_k^m| \equiv \sum_{m=1}^{4}\hat{V}_m\,|\Gamma_k^m|, \tag{5}$$

$$(v_i^{n+1})_k = (\hat{v}_i)_k - \frac{1}{|\Omega_k|}\sum_{m=1}^{4}\Psi_m \cdot {}^i n_k^m\,|\Gamma_k^m|, \tag{6}$$

$$(p^{n+1})_k = (p^n)_k + \frac{1}{\Delta t}(\Psi)_k, \tag{7}$$

$$V_m^{n+1} = \hat{V}_m - \frac{\partial\Psi}{\partial \boldsymbol{n}_k^m}\,, \tag{8}$$

where Δt is the time step, $|\Omega_k|$ is the volume of the control volume Ω_k, $k = 1, \ldots, N_{CV}$, Fig. 8, $(\Phi)_k = \frac{1}{|\Omega_k|}\int_{\Omega_k}\Phi \mathrm{d}\Omega$ is the integral average for an arbitrary flow quantity Φ over control volume Ω_k, $|\Gamma_k^m|$, $m = 1, \ldots, 4$ is the area of the m-th face Γ_k^m of the control volume Ω_k, ${}^i n_k^m$ is the i-th component of the outward unit vector $\boldsymbol{n}_k^m = [{}^1 n_k^m, {}^2 n_k^m, {}^3 n_k^m]^T$ normal to the face Γ_k^m and $\hat{V}_m = \hat{v}_{im}\cdot {}^i n_k^m$ denotes the intermediate face-normal velocity at the face Γ_k^m. Note that the values of face-normal velocity V_m^{n+1} computed with the help of Eq. (8) are used as values of face-normal velocity V_m^n in Eq. (3) at the next time level. For the determination of values $\delta\hat{v}_{i\,m}$, $v_{i\,m}^n$, p_m^n, Ψ_m and derivatives $\frac{\partial\Psi}{\partial \boldsymbol{n}_k^m}$, $\frac{\partial}{\partial \boldsymbol{n}_k^m}\left(\delta\hat{v}_{i\,m} + 2v_{i\,m}^n\right)$ at the m-th face Γ_k^m of the control volume Ω_k, the application of an interpolation method is used. For more details on the described numerical method, see Vimmr et al.[11] In relation to paper's objectives to model pulsatile blood flow, boundary conditions are prescribed as

- inlet $\Gamma_k^m \subset \partial\Omega_I$: $v_{i\,m} = v_{i\,I}$, $\left.\frac{\partial v_{i\,m}}{\partial \boldsymbol{n}_k^m}\right|_{\Gamma_k^m} = 0$, $\left.\frac{\partial\Psi}{\partial \boldsymbol{n}_k^m}\right|_{\Gamma_k^m} = 0$, where the inlet velocity vector components $v_{i\,I}$ are given in non-dimensional form for corresponding inlet boundaries of both bypass models, see Sec. 2;
- outlet $\Gamma_k^m \subset \partial\Omega_O$: $p_m \boldsymbol{n}_k^m - \frac{1}{\mathrm{Re}^{(s)}}\frac{\partial \boldsymbol{v}_m}{\partial \boldsymbol{n}_k^m} = p_O \boldsymbol{n}_k^m$, $\Psi_m = 0$, where p_O is the prescribed non-dimensional value of outlet pressure, see Sec. 2;
- rigid wall $\Gamma_k^m \subset \partial\Omega_W$: $v_{i\,m} = 0$, $\left.\frac{\partial\Psi}{\partial \boldsymbol{n}_k^m}\right|_{\Gamma_k^m} = 0$.

The solution of Eq. (3) leads to a system of linear algebraic equations $\mathbf{A}_{NS} \cdot \mathbf{x}_{NS} = \mathbf{b}_{NS}$ for $3 \cdot N_{CV}$ unknown values $(\delta\hat{v}_i)_k$, $i = 1, 2, 3$, $k = 1, 2, \ldots N_{CV}$, where N_{CV} is the number of control volumes within the hybrid unstructured computational mesh. Similarly, the solution of Poisson equation (5) for the pressure correction function leads to a system of linear algebraic equations $\mathbf{A}_{Poi} \cdot \mathbf{x}_{Poi} = \mathbf{b}_{Poi}$ for N_{CV} unknown values $(\Psi)_k$, $k = 1, 2, \ldots N_{CV}$. Since both systems of equations contain large sparse matrices $\mathbf{A}_{NS}$ and $\mathbf{A}_{Poi}$, it is favourable to use an iterative solution. In our case, BICGSTAB method with incomplete LU preconditioner is applied. This kind of methods is a standard part of the MATLAB software. For the incomplete LU decomposition, the UMFPACK library is used.

4 NUMERICAL RESULTS, DISCUSSION AND CONCLUSIONS

Let us note that in this section all numerical results are presented in their dimensional form. For the case of individual aorto-coronary bypass, Fig. 9–10 show velocity vectors at both the proximal and distal anastomoses at two time instants $t_1 = 0.055\,\mathrm{s}$ and $t_2 = 0.095\,\mathrm{s}$, respectively. The position of both pre-systolic time instants within the the cardiac cycle at the aorta is denoted in Fig. 4 for the values of inlet flow rate and outlet pressure. In the case of proximal anastomosis, the presence of a 'bulge' filled with a weak recirculation zone seems to significantly affect velocity distribution and consequently the blood supply to the distal anastomosis. Moreover, the present shape of the proximal junction region and its close proximity to high-velocity aorta may enhance the risk of thrombus formation due to the possibility of blood cells accumulation and platelet activation. Regarding the distal anastomosis of the individual bypass model, the flow distribution between the pre- and

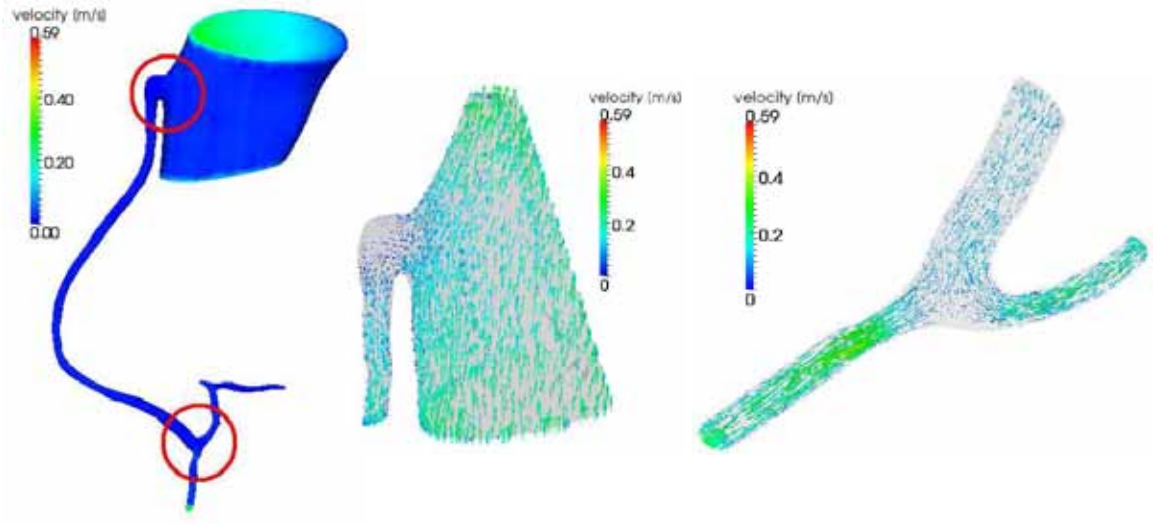

Figure 9: Velocity distribution within the individual aorto-coronary bypass model and velocity vectors at the proximal end-to-side and distal end-to-side anastomoses at the time $t_1 = 0.055\,\mathrm{s}$

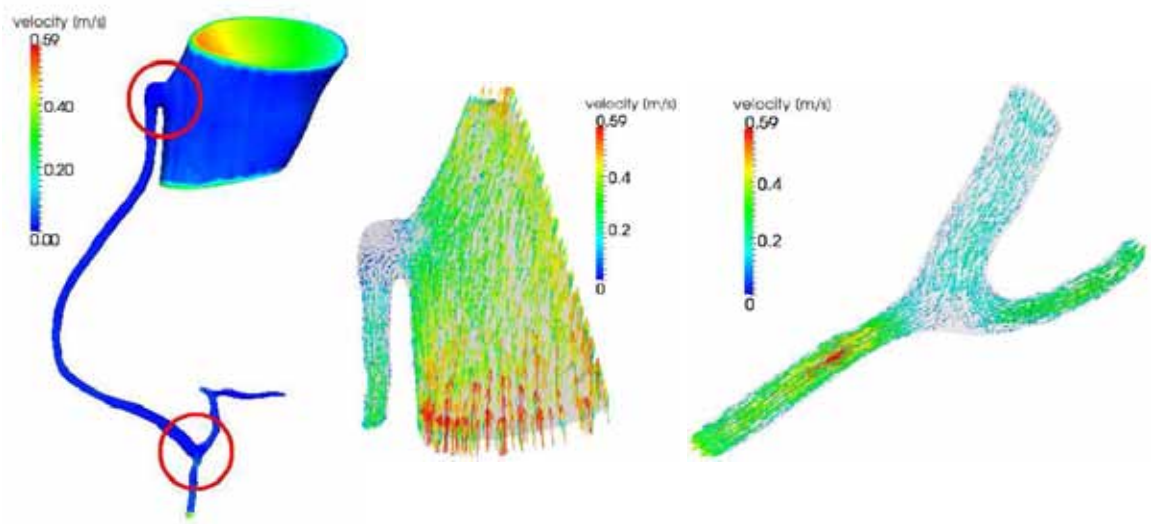

Figure 10: Velocity distribution within the individual aorto-coronary bypass model and velocity vectors at the proximal end-to-side and distal end-to-side anastomoses at the time $t_2 = 0.095\,\mathrm{s}$

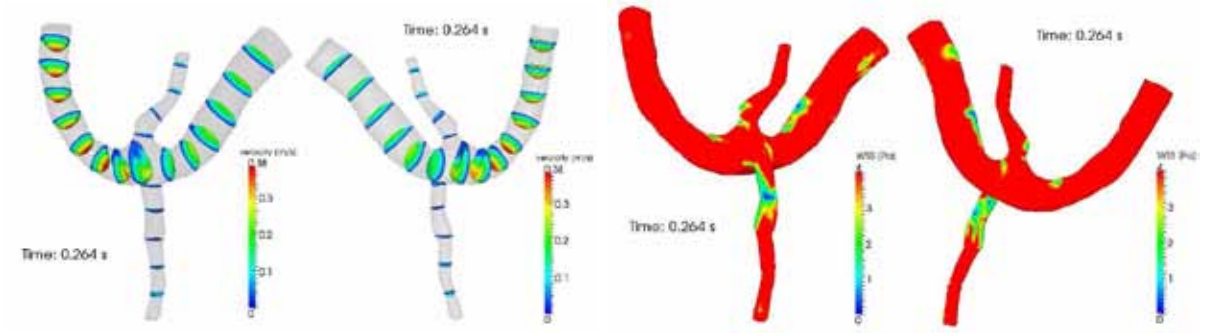

Figure 11: Side-to-side anastomosis – selected velocity profiles (*left*) and corresponding WSS distribution (*right*) at the time $t_1 = 0.264\,\mathrm{s}$

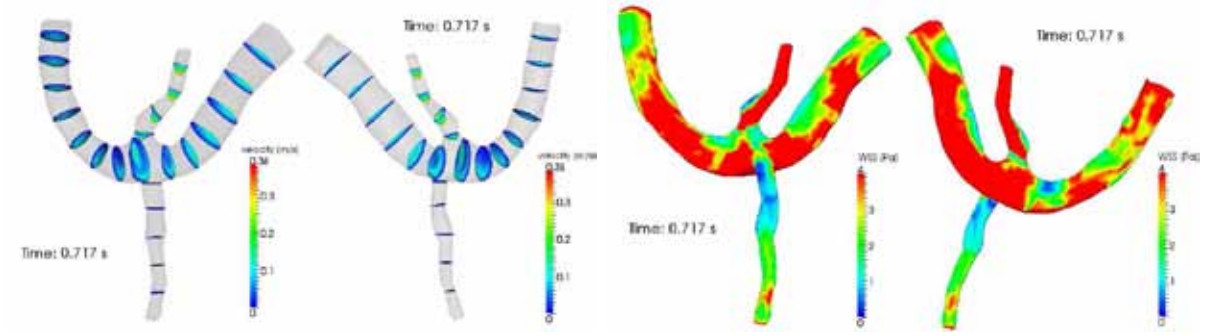

Figure 12: Side-to-side anastomosis – selected velocity profiles (*left*) and corresponding WSS distribution (*right*) at the time $t_2 = 0.717\,\mathrm{s}$

$$\mathrm{OSI} = \frac{1}{2}\left(1 - \frac{\left|\int_0^T \boldsymbol{\tau}_W \,\mathrm{d}t\right|}{\int_0^T |\boldsymbol{\tau}_W| \,\mathrm{d}t}\right)$$

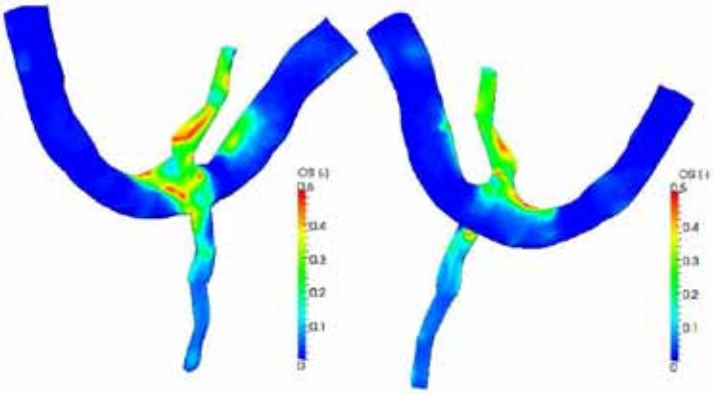

Figure 13: Formula used for the calculation of oscillatory shear index (OSI)[12] and OSI distribution at the side-to-side anastomosis

post-anastomosis branch of the coronary artery appears to be relatively uniform. However, due to this kind of stream division, blood remains almost motionless in a certain part of the anastomosis near the arterial floor, which may prove to be a significant trigger of intimal hyperplasia in this bypass model.

In relation to numerical simulation of pulsatile blood flow in the side-to-side anastomosis model, velocity profiles at selected cross-sections with corresponding WSS distributions are shown in Fig. 11–12 for two time instants $t_1 = 0.264\,\mathrm{s}$ and $t_2 = 0.717\,\mathrm{s}$, respectively. The time instants correspond either to systolic or diastolic phases of the cardiac cycle, see Fig. 7. Since low WSS values are of main interest when dealing with intimal hyperplasia, WSS distributions in Fig. 11–12 are displayed for a lowered range $(1 - 4\,\mathrm{Pa})$. The results indicate a considerably non-uniform WSS stimulation of all bypass walls, especially in the anastomosis region. This assumption is supported by the skewed shape of velocity profiles in this area during systole, Fig. 11. Moreover, according to calculated WSS values, blood supply to the coronary artery downstream from the anastomosis seems to be taking place only before diastole. The influence of pulsatile blood flow on arterial wall stimulation in relation to intimal hyperplasia development is usually recorded in the form of oscillatory shear index[12]. The formula for its calculation and corresponding distribution at the side-to-side anastomosis model is shown in Fig. 13, where OSI values equal to 0.5 indicate a highly oscillating WSS and at the same time denote a bypass area prone to intimal thickening.

ACKNOWLEDGMENTS

This investigation was supported by the European Regional Development Fund, project "NTIS – New Technologies for Information Society", European Centre of Excellence, CZ.1.05/1.1.00/02.0090 and by the research project MSM 4977751303 of the Ministry of Education, Youth and Sports of the Czech Republic.

REFERENCES

[1] *European Cardiovascular Disease Statistics - 2008 Edition*. European Heart Network, (2008), Oxford, UK.

[2] Haruguchi, H. and Teraoka, S. Intimal hyperplasia and hemodynamic factors in arterial bypass and arteriovenous grafts: A review. *J. Artif. Organs* (2003) **6**:227–235.

[3] Loth, F., Fischer, P.F. and Bassiouny, H.S. Blood flow in end-to-side anastomoses. *Annu. Rev. Fluid Mech.* (2008) **40**:367–393.

[4] Malek, A.M. and Izumo, S. Mechanism of endothelial cell shape change and cytoskeletal remodelling in response to fluid shear stress. *J. Cell Sci.* (1996) **109**:713–726.

[5] Bertolotti, C., Deplano, V., Fuseri, J. and Dupouy, P., Numerical and experimental model of post-operative realistic flows in stenosed coronary bypasses. *J. Biomech.* (2001) **34**:1049-1064.

[6] Friedman, M.H., Bargeron, C.B., Duncan, D.D., Hutchins, G.M. and Mark, F.F. Effects of arterial compliance and non-Newtonian rheology on correlations between intimal thickness and wall shear. *J. Biomech. Eng.* (1992) **114**:317–320.

[7] Vimmr, J. and Jonášová, A. Non-Newtonian effects of blood flow in complete coronary and femoral bypasses. *Math. Comput. Simulat.* (2010) **80**:1324–1336.

[8] Olufsen, M.S., Peskin, C.S., Kim, W.Y., Pedersen, E.M., Nadim, A. and Larsen, J. Numerical simulation and experimental validation of blood flow in arteries with structured-tree out?ow conditions. *Ann. Biomed. Eng.* (2000) **28**:1281–1299.

[9] Frauenfelder, T., Boutsianis, E., Schertler, T., Husmann, L., Leschka, S., Poulikakos, D., Marincek, B. and Alkadhi, H. Flow and wall shear stress in end-to-side and side-to-side anastomosis of venous coronary artery bypass grafts. *BioMedical Engineering OnLine* (2007) **6**:1–13. (doi:10.1186/1475-925X-6-35)

[10] Kim, D. and Choi, H. A second-order time-accurate finite volume method for unsteady incompressible flow on hybrid unstructured grids. *J. Comput. Phys.* (2000) **162**:411–428.

[11] Vimmr, J., Jonášová, A. and Bublík, O. Effects of three geometrical parameters on pulsatile blood flow in complete idealized coronary bypasses. *Comput. Fluids* (2011). (preprint submitted in March 2011)

[12] Ku, D.N., Giddens, D.P., Zarins, C.K. and Glagov, S. Pulsatile flow and atherosclerosis in the human carotid bifurcation - Positive correlation between plaque location and low oscillating shear stress. *Arterioscl. Throm. Vas.* (1985) **5**:293–302.